ACS APPLIED MATERIALS & INTERFACES

Research Article

www.acsami.org

$CH_3NH_3PbI_3$-Based Planar Solar Cells with Magnetron-Sputtered Nickel Oxide

Jin Cui,[†] Fanping Meng,[‡] Hua Zhang,[†] Kun Cao,[†] Huailiang Yuan,[†] Yibing Cheng,[†,§] Feng Huang,*[,‡] and Mingkui Wang*[,†]

[†]Michael Grätzel Centre for Mesoscopic Solar Cells, Wuhan National Laboratory for Optoelectronics, Huazhong University of Science and Technology, Wuhan, 430074 Hubei, People's Republic of China

[‡]Ningbo Institute of Materials Technology and Engineering, Chinese Academy of Sciences, Ningbo, 315201 Zhejiang, People's Republic of China

[§]Department of Materials Engineering, Monash University, Melbourne, Victoria 3800, Australia

Supporting Information

ABSTRACT: Herein we report an investigation of a $CH_3NH_3PbI_3$ planar solar cell, showing significant power conversion efficiency (PCE) improvement from 4.88% to 6.13% by introducing a homogeneous and uniform NiO blocking interlayer fabricated with the reactive magnetron sputtering method. The sputtered NiO layer exhibits enhanced crystallization, high transmittance, and uniform surface morphology as well as a preferred in-plane orientation of the (200) plane. The PCE of the sputtered-NiO-based perovskite p–i–n planar solar cell can be further promoted to 9.83% when a homogeneous and dense perovskite layer is formed with solvent-engineering technology, showing an impressive open circuit voltage of 1.10 V. This is about 33% higher than that of devices using the conventional spray pyrolysis of NiO onto a transparent conducting glass. These results highlight the importance of a morphology- and crystallization-compatible interlayer toward a high-performance inverted perovskite planar solar cell.

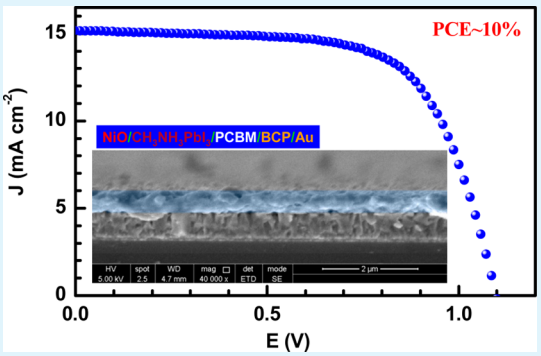

KEYWORDS: *solar cell, perovskite, NiO blocking layer, magnetron sputtering, solvent engineering*

INTRODUCTION

Solar energy is one of the biggest energy sources of the future. Clearly, the efficiency of solar cells depends heavily upon the light absorbers. The organometallic halide pervoskite-based solar cell is a new type of photovoltaic with power conversion efficiency (PCE) currently exceeding 19%.[1] $CH_3NH_3PbI_3$ is an ideal optoelectronic material that exhibits a direct optical band gap of around 1.5 eV with a high extinction coefficient ($\sim 10^4$ cm^{-1}), low exciton bonding energy (0.01 eV), and long diffusion length ($\sim$0.1–1 μm).[2−5] It has been reported that $CH_3NH_3PbI_3$ shows ambipolar characteristics and works well with various organic carrier transport materials, including 2,2′7,7′-tetrakis(*N*,*N*-bis(*p*-methoxyphenyl)amino)-9,9′-spirobifluorene,[6] fullerene (C60), [6,6]-phenyl C61-butyric acid methyl ester (PCBM),[7−9] and other conjugated polymers,[10−12] to form hybrid heterojunctions. Since Snaith et al. first reported the work of the inverted perovskite planar solar cells by deposition of a p-type-selective contact onto the FTO/glass substrate,[8] more and more researchers have become interested in this type of device.

In a perovskite planar solar cell, the electron–hole pair by photoexcitation could separate after thermalization through two possible primary processes: (1) injection of electrons into electron-selective materials such as PCBM and/or (2) injection of holes into hole-selective materials such as nickel oxide (NiO). Poly(3,4-(ethylenedioxy)thiophene)/poly-(styrenesulfonate) (PEDOT/PSS) has been widely used as an electron-blocking layer (EBL) in perovskite planar solar cells, achieving outstanding photovoltaic performance (~15%).[13] However, researchers are aware of the drawbacks from the PEDOT/PSS interlayer being unstable.[14−16] Therefore, NiO has been selected to be incorporated into these devices as a hole conductor. NiO is a cubic wide band gap p-type semiconductor which is essentially transparent for very thin layers and can act as an electron-blocking interlayer. Irwin et al. first reported the replacement of the PEDOT/PSS layer by a thin NiO layer in polymer bulk-heterojunction solar cells, resulting in an enhanced device efficiency in photocurrent and fill factor.[17] Chen et al. reported the outstanding work of the efficient $CH_3NH_3PbI_3$/PCBM heterojunction using NiO_x as the electron-blocking layer. The energy level at the junction interfaces was intensively investigated, aiming for a favorable

Received: October 15, 2014
Accepted: November 26, 2014
Published: November 26, 2014

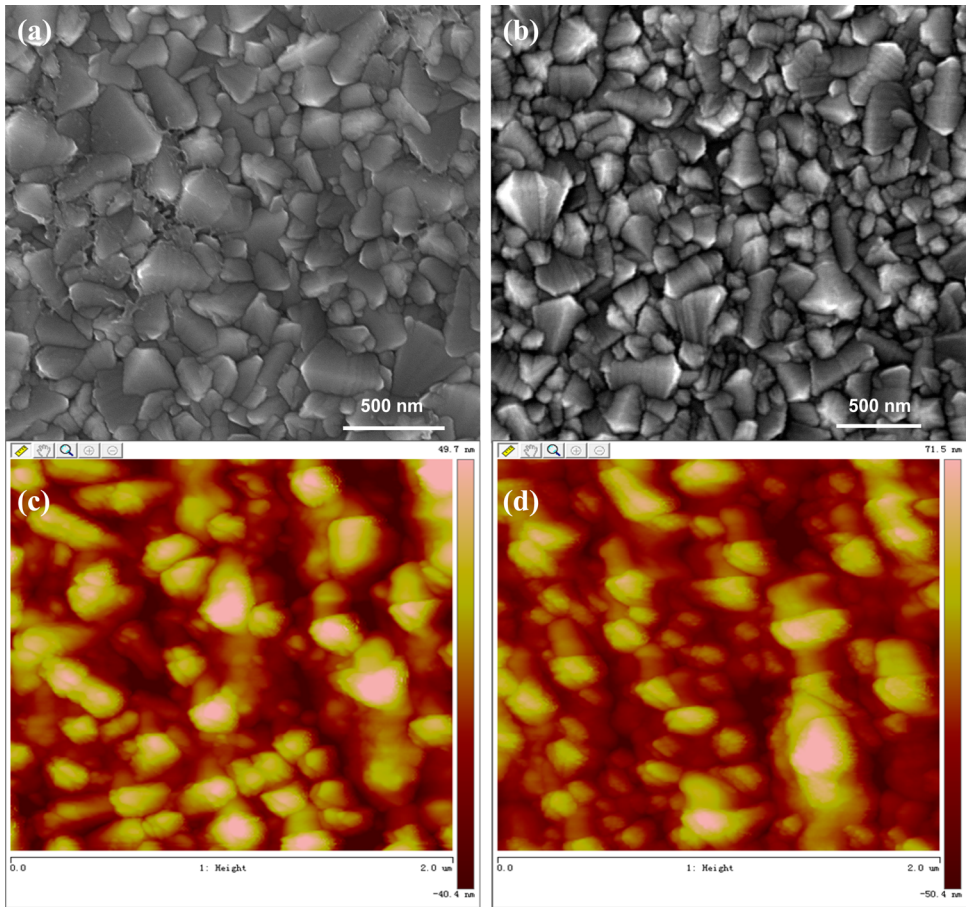

Figure 1. Top-view FE-SEM images of NiO compact layers fabricated on FTO electrodes by using (a) RMS and (b) spray pyrolysis methods. The average thickness of the NiO film is about 50 nm in each sample. The corresponding AFM images are shown in (c) and (d). The root-mean-square roughness values can be estimated from NanoScope Analysis software.

charge transfer at different interfaces and achieving a PCE of 7.8% by using NiO_x as the p-contact electrode material.[18] This is the highest efficiency so far for the NiO-based perovskite planar solar cell.

Since NiO deposition is usually the very beginning step during the device construction, the optimization of morphology and crystallization becomes obviously important for formation of a homogeneous and uniform electron-blocking layer. In this work, to fabricate efficient NiO/$CH_3NH_3PbI_3$/PCBM planar solar cells, a reactive magnetron sputtering (RMS) method was introduced to prepare a NiO compact layer on FTO electrodes. RMS can be operated at a low deposition temperature and high deposition rate, which produces highly dense films. A solvent-engineering technology for $CH_3NH_3PbI_3$ formation was further applied to prepare homogeneous surface coverage and uniform active layers. A planar cell with the FTO/NiO/$CH_3NH_3PbI_3$/PCBM/BCP/Au configuration presents an impressive open circuit voltage (V_{oc}) of 1.10 V, a short-circuit current (J_{sc}) of 15.17 mA cm^{-2}, and a fill factor (FF) of 0.59, corresponding to a PCE of 9.84% under standard 1 sun AM 1.5G simulated solar irradiation. Compared to the work from Chen et al.,[18] this work not only shows the optimization of the preparation method of the NiO layer and perovskite layer, but also emphasizes the importance of a morphology- and crystallization-compatible interlayer toward a high-performance inverted perovskite planar solar cell. Our results point out a method to fabricate efficient perovskite planar solar cells with a NiO electrode as the electron-blocking interlayer.

EXPERIMENTAL SECTION

Materials and Sample Preparation. The ethylammonium lead iodide ($CH_3NH_3PbI_3$) was prepared according to other reports.[5] The solar cell devices were fabricated in a standard arrangement by sandwiching an active layer of $CH_3NH_3PbI_3$ between a NiO electron-blocking underlayer and a PCBM electron-extracting layer. The counter electrode was made of a bathocuproine (BCP) (Aldrich) film (as an exciton-blocking layer) and gold (Au). Prior to the device fabrication, the etched substrate was cleaned with 2% Hellmanex diluted in Milli-Q water, rinsed with Milli-Q water and ethanol, and dried with clean dry air. The substrate was treated in a UV-O_3 chamber for 30 min prior to NiO compact layer deposition. The $CH_3NH_3PbI_3$ precursor solution was prepared by mixing CH_3NH_3I with PbI_2 in a 1:1 molar ratio (0.8 g:2.3 g) in 4.7 mL of anhydrous *N*,*N*-dimethylformamide (Aldrich) (40 wt % solution) at 60 °C, stirring for 12 h inside a nitrogen-filled glovebox with oxygen and moisture levels of <1 ppm. Syringe dispensing of 100 μL of toluene during spin coating of the $CH_3NH_3PbI_3$ precursor (5000 rpm for 30 s) ensures $CH_3NH_3PbI_3$ formation in a fast regime to inhibit coarsening of the crystals. The thickness of the $CH_3NH_3PbI_3$ layer was approximately 240 nm as determined by the cross session images of scanning electron microscopy (SEM). The PCBM (~60 nm) and BCP (<10 nm) were spin-coated (1500 rpm for 30 s and 2000 rpm for 45 s, respectively) inside a nitrogen-filled glovebox. The Au electrode (65 nm) was thermally deposited on the BCP layer inside a vacuum chamber (10^{-6} Torr).

Fabrication of the NiO Electrode Interlayer. The NiO thin films were reactively deposited on the precleaned and prepatterned FTO substrates. Details of the sputtering apparatus have been described in previous work.[19] Briefly, the Ni target was driven by a radio frequency (rf; Comdel CV-1000, 81 MHz) power supply at 300 W, yielding a ~2 nm/min deposition rate. Prior to deposition, the base pressure was pumped down to $<5 \times 10^{-4}$ Pa. Pure oxygen was used as the sputter gas with a total 0.5 Pa of pressure. The substrates were not intentionally heated. NiO films with different thicknesses were obtained by adjusting the growth time.

For comparison, spray pyrolysis was performed using 0.2 mol L^{-1} nickel acetylacetonate in acetonitrile.[20] The substrate was heated from room temperature to 450 °C in 30 min. The spray was purged out through a spraying head with an oxygen flow. The carrier gas was adjusted by a regulation valve, and the spray was controlled by a ball valve being turned on and off to deliver a stable flow. The sprayed layer was left at 450 °C for 15 min and allowed to cool to room temperature.

Characterization. The current density−voltage characteristics of the devices were measured using a Keithley 2400 digital source meter under simulated AM 1.5G solar irradiation at 100 mW cm^{-2} (Newport, AAA solar simulator, 94023A-U) in the air. The $J-V$ characteristics were recorded by reverse scan or forward scan in the range from −0.1 to +1.3 V with a scan rate of 10 mV s^{-1}. The shunt resistance (R_{sh}) of the devices was estimated from the $J-V$ testing results with a basic diode equivalent circuit model.[21] Ultraviolet photoemission spectroscopy (UPS) measurement was carried out in a Kratos AXIS Ultra-DLD ultra-high-vacuum photoemission spectroscopy system with an Al Kα radiation source. Tapping mode atomic force microscopy (AFM) was performed using a Veeco multimode instrument. SEM images were obtained using an FEI Nova NanoSEM 450. X-ray diffraction (XRD) results were acquired using a Phillips X'Pert PRO. The electronic impedance spectroscopy (IS) measurement of the devices was carried out under white LED illumination of 10 mW cm^{-2} with an Autolab frequency analyzer setup, which consists of an Autolab PGSTAT 30 (Eco Chemie B.V., Utrecht, The Netherlands) producing a small-amplitude harmonic voltage and a frequency response analyzer module.

RESULTS AND DISCUSSION

In this study, for a systematic comparison of the effect of the electron-blocking interlayer on the device photovoltaic performance, a NiO thin film was deposited onto the patterned FTO with the RMS and spray pyrolysis techniques. Both methods have been widely used in thin film fabrication (for details see the Experimental Section). FTO substrates consist of F-doped SnO_2 grains with particle size ranging from tens to hundreds of nanometers. Owing to the grain boundaries, the FTO substrate shows a rough surface. FTO glass was selected due to the requirement of a high-temperature process for the spray method. Parts a and b of Figure 1 present SEM images of the NiO layer on FTO substrates fabricated with the RMS and spray pyrolysis methods, respectively. Due to a very small thickness (about 50 nm), the NiO thin layer surface morphologies predominantly replicate the underlying FTO relief morphology, except for the wrinkles caused by very small NiO particles. A further AFM characterization shows that the in situ deposition processes significantly planarize the anode surface, evidenced by reducing the root-mean-square roughness of 27−28 nm for the bare FTO glass to 20−21 and 24−25 nm for the FTO/NiO sample with the RMS method and spray pyrolysis method (Figure 1c,d). The presence of crystalline NiO was confirmed by glancing-angle X-ray diffraction (GA-XRD). Figure 2 presents the XRD for both NiO films. The samples were intentionally fabricated onto a flat glass substrate with a controlled thickness of 100 nm for XRD intensity

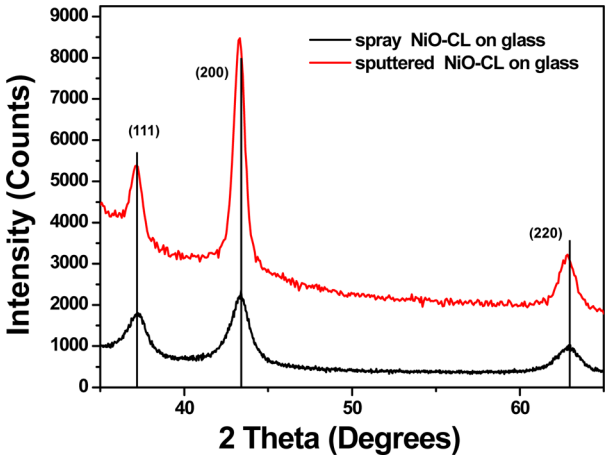

Figure 2. Glancing-angle X-ray diffraction patterns of 100 nm thick NiO films grown on flat glass substrates with RMS (red curve) and spray pyrolysis (black curve) methods. Features are labeled with the corresponding (*hkl*) reflections of cubic-phase NiO.

comparison. As shown in Figure 2, the characteristic NiO reflections are clearly visible. The sputtered NiO layer exhibits a more preferential in-plane orientation of the (200) plane. It is noted that sputtered NiO shows better crystallinity (Figure 2) and greater grain size (Figure S1, Supporting Information) than sprayed NiO.

NiO films with different thickness from 10 to 100 nm were deposited for comparison. As shown in Figure 3, the NiO layers

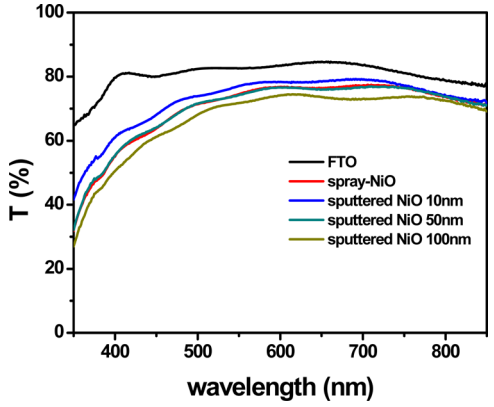

Figure 3. Optical transmission spectra of NiO films grown on FTO with RMS and spray pyrolysis methods. The black curve was obtained with the FTO glass.

with 10−50 nm thickness were found to be highly transparent (>75%) in the range from 450 to 750 nm. The high transparency allows a large photon flux to reach the $CH_3NH_3PbI_3$ layer for photocurrent generation. However, it was found that the devices with a 10 nm sputtered NiO electrode interlayer showed reduced photovoltaic performance (Table S1, Supporting Information), which might be caused by the unsatisfactory coverage of the thin NiO film (~10 nm) on the FTO substrates. It was further found that the intrinsic photon absorption by NiO was likely to be the dominant factor affecting the device performance when 50 and 100 nm thick sputtered NiO was used. Therefore, we chose the sputtered NiO film with 50 nm thickness for device fabrication in the following discussion.

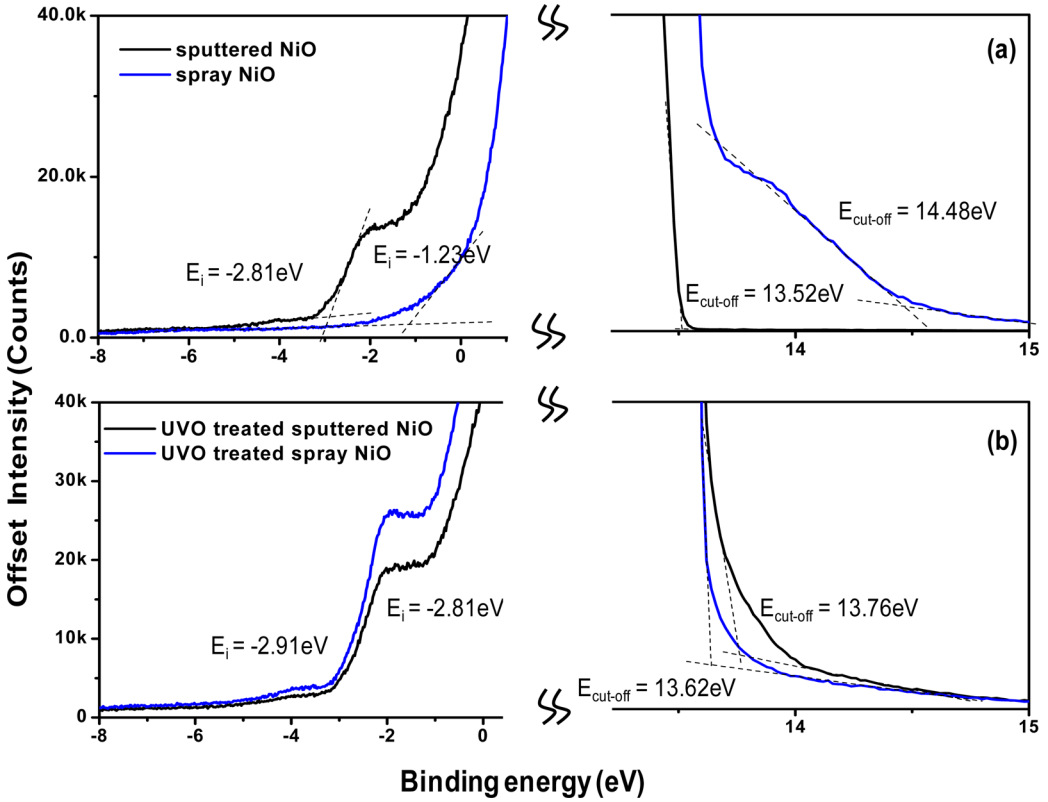

Figure 4. UPS spectra in the onset (E_i) and the cutoff (E_{cutoff}) energy regions of the surface measurement for the glass/FTO/sputtered NiO (black curve) and glass/FTO/sprayed NiO (blue curve) substrates (a) and the UVO-treated samples (b).

UV-ozone (UVO) treatment for 3 min can modify the work function and surface wetting properties of the NiO layer.[16] Figure 4 depicts the onset (E_i) and cutoff (E_{cutoff}) energy regions in the UPS spectrum (He I) for the FTO/sputtered NiO and FTO/sprayed NiO samples before and after UVO treatment. As shown in Figure 4a, the work function (φ) of sputtered and sprayed NiO interlayers before UVO treatment was estimated to be 4.9 and 5.5 eV (vs vacuum) with the equation $\varphi = 21.21 - (E_{cutoff} - E_i)$. The valence band (VB) maximum of NiO is reported to be 0.4 eV below the hole Fermi level (E_f) of this semiconductor.[22,23] The VB energy difference of sputtered and sprayed NiO might be ascribed to the effect of vacuum annealing of sputtered NiO. This procedure makes NiO highly defective with oxygen vacancies, resulting in the Fermi level position of the oxide moving away from the valence band maximum and decreasing the work function.[24] Therefore, the VB energy levels of sputtered and sprayed NiO can be estimated to be −5.3 and −5.9 eV, respectively. These values indicate that hole injection from the $CH_3NH_3PbI_3$ into the sprayed NiO sample might not be efficient due to a VB at −5.4 eV for the light absorber (Figure S2b, Supporting Information). Interestingly, the UVO treatment induces an obvious shift of the NiO layer VB with respect to the $CH_3NH_3PbI_3$ to a matched level (φ = ∼4.68 eV, VB at ∼−5.08 eV) by doping of surface oxygen defects and surface cleaning.[25,26] Figure S2b diagrams the energy level of each individual functional layer. The conduction band (CB) (−3.9 eV) and VB (−5.4 eV) edge energy levels in $CH_3NH_3PbI_3$ exhibit good alignment with the LUMO level of PCBM (−3.9 eV) and the VB of NiO (−5.1 eV), respectively. The holes transfer from the $CH_3NH_3PbI_3$ layer to the Ni^{2+} vacancy-based (excess O) hole-conducting NiO band. However, the highly defective oxygen vacancies would cause the Fermi level position of NiO to move away from the valence band maximum, which would minimize the energy level difference between NiO and perovskite. A tiny energy loss for charge carrier (electron and hole) transfer at the $CH_3NH_3PbI_3$/PCBM and NiO/$CH_3NH_3PbI_3$ interfaces can enhance the photovoltage output. Meanwhile, NiO is a wide band gap material with a CB edge level around −2.1 eV, which is much higher than that of $CH_3NH_3PbI_3$ at around −3.9 eV; thus, injection of an electron from $CH_3NH_3PbI_3$ into NiO is not energetically favorable.

The electron-blocking function of the compact NiO layers in the devices was first investigated by fabrication of a group of NiO/$CH_3NH_3PbI_3$/PCBM planar solar cells under identical conditions, except the NiO compact layers. A reference cell without a compact NiO layer was also fabricated for comparison. The NiO layer was first evaluated in devices with $CH_3NH_3PbI_3$ formed with a conventional solution-processed method.[18] Figure S2a (Supporting Information) illustrates a device with the FTO/NiO/$CH_3NH_3PbI_3$/PCBM/BCP/Au configuration. The J−V curves of devices from each group are shown in Figure 5a, and the corresponding photovoltaic parameters are summarized in Table 1. The device without a blocking layer yielded low photovoltaic performance along with negligible J_{sc}, V_{oc}, and FF as shown in Table 1. This was caused by the intimate contact between the FTO and perovskite and/or PCBM. In contrast, after a blocking layer was introduced, for example, by spray pyrolysis, the device's performance was significantly improved, exhibiting a J_{sc} of 11.46 mA cm^{-2} and V_{oc} of 0.98 V together with an FF of 0.43, indicating the importance of the electron-blocking layer in the device. The performance was further improved by using sputtered NiO layers. The device with a sputtered NiO

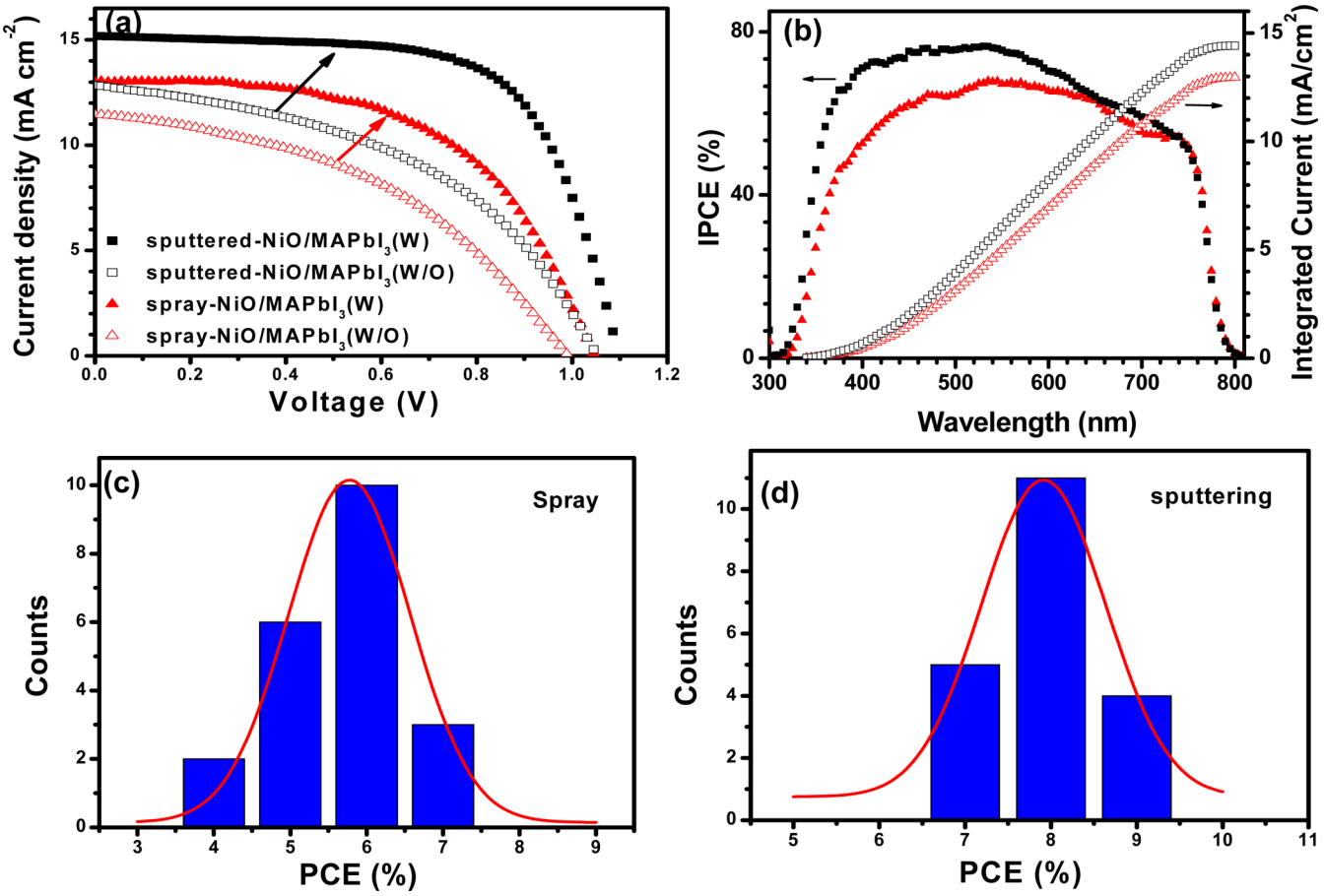

Figure 5. J–V curves (a) and IPCE spectra (b) of devices with (■) FTO/sputtered NiO/$CH_3NH_3PbI_3$(W)/PCBM/BCP/Au and (▲) FTO/sprayed NiO/$CH_3NH_3PbI_3$(W)/PCBM/BCP/Au. Histograms c and d show the efficiencies of different cell groups measured from 21 devices. The open symbols (△, □) are for the corresponding devices with conventional solution-processed $CH_3NH_3PbI_3$. W indicates a $CH_3NH_3PbI_3$ film prepared with the solvent-engineering process.

Table 1. Photovoltaic Parameters of the NiO/$CH_3NH_3PbI_3$/PCBM Planar Solar Cells

blocking layer	solution process	V_{oc} (V)	J_{sc} (mA/cm^2)	FF	PCE (%)	R_{sh} (Ω cm^2)	R_s (Ω cm^2)
sputtered NiO	normal one-step process	1.05	12.93	0.45	6.13	5432.2	315.5
sprayed NiO		0.98	11.46	0.43	4.88	4449.1	468.9
none		0.39	1.03	0.22	0.09	3955	5576
sputtered NiO	solvent-engineering technology	1.10	15.17	0.59	9.84	57244	85.5
sprayed NiO		1.01	13.54	0.54	7.39	35860	241

compact layer showed simultaneous improvement in all parameters, with a high J_{sc} of 12.93 mA cm^{-2}, a high V_{oc} of 1.05 V, and a good FF of 0.45, resulting in a decent PCE of 6.13%. The performance improvement gave direct evidence of sputtered NiO as an outstanding electron-blocking layer in the NiO/$CH_3NH_3PbI_3$/PCBM planar structure device. Compared to the reported data on this structure, the device in this study showed a relatively low fill factor. Detailed investigation found that the limited photovoltaic performance could be due to poor $CH_3NH_3PbI_3$ film formation upon the NiO substrate and surface coverage as shown in Figure 6a, which causes a shunting path in the devices. From the cross-sectional SEM image of the $CH_3NH_3PbI_3$ film on NiO (Figure 6c), we can see a rough layer with accidented grains, which has a significant influence on the PCBM coverage.

Therefore, a solvent-engineering technology was introduced to gain further insight into the importance of a morphology- and crystallization-compatible interlayer toward performance in planar devices.[27,28] The solvent-engineering technology highly improved the photovoltaic performance of devices with a sputtered NiO electrode. Figure 6b presents the SEM image of the top view of $CH_3NH_3PbI_3$ fabricated with solvent-engineering technology (see the Experimental Section), showing a high surface coverage and uniform film compared with that obtained by the conventional solution-processed method. It is well-known that the crystal growth and aggregation of $CH_3NH_3PbI_3$ during the spin-coating process coarsen the films on the substrate and may degrade the devices' performance or result in device failure. Seok et al. have shown the important role of solution processing in the realization of highly efficient perovskite solar cells.[29] We found in this study that dispensation of toluene onto the rotating film at a high spinning speed of 5000 rpm during the solvent (DMF) evaporation process can be helpful for $CH_3NH_3PbI_3$ crystal formation in a short time regime and inhibition of the coarsening of the crystals. Figure 5a presents the devices'

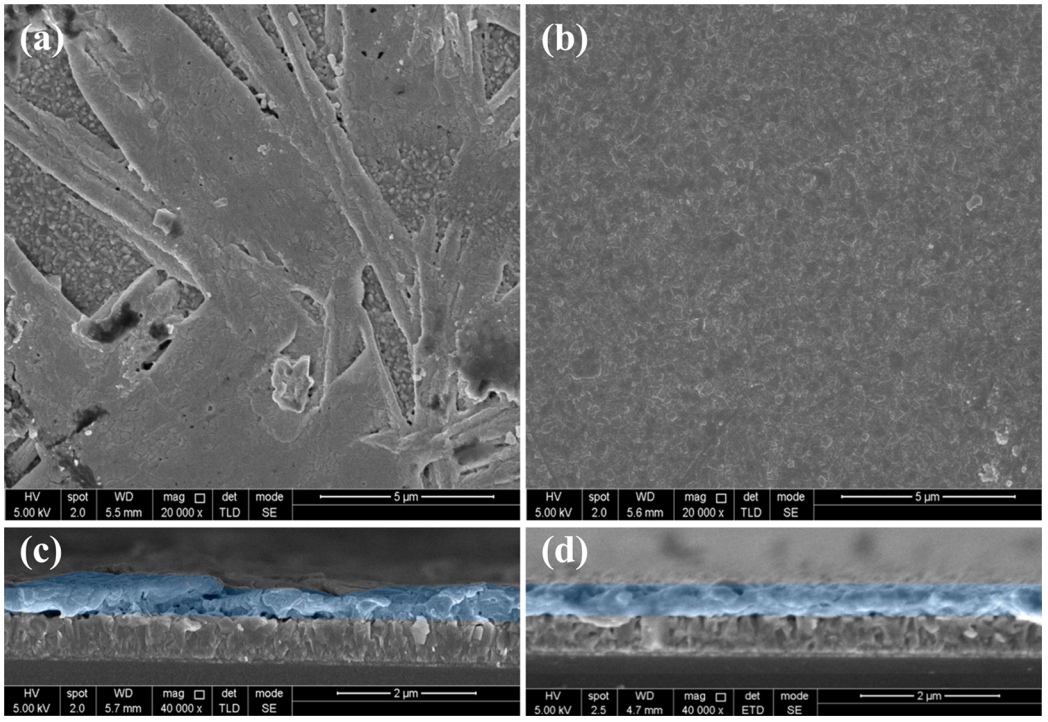

Figure 6. Top-view and cross-sectional SEM images of the $CH_3NH_3PbI_3$ perovskite film surface prepared by the conventional one-step precursor deposition method (a, c) and solvent-engineering one-step precursor deposition method (b, d). The ratio of surface coverage for images a and b estimated by ImageJ software is estimated to be approximately 67% and 96%, respectively.

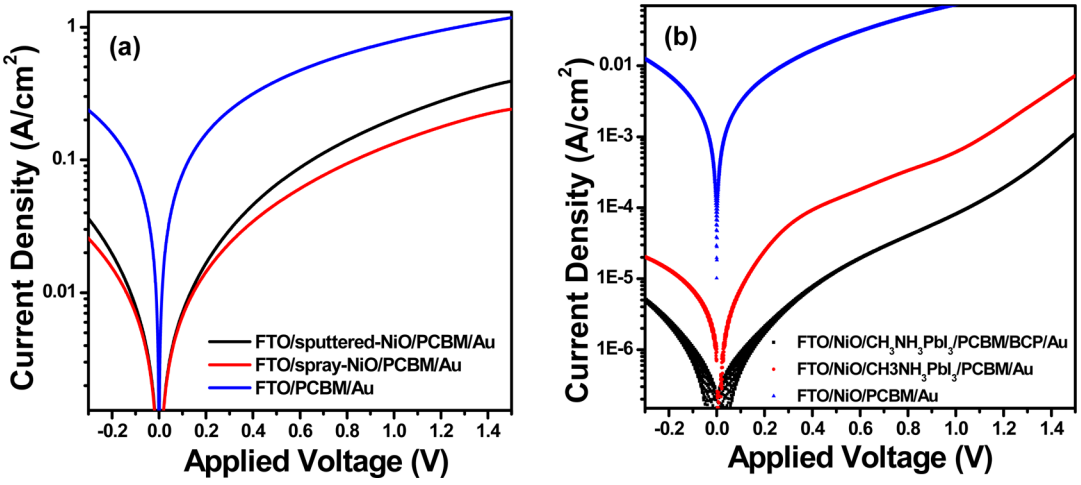

Figure 7. Leakage current test of the simplified device structure: (a) FTO/electron-blocking layer/PCBM/Au electrode and (b) FTO/$CH_3NH_3PbI_3$/PCBM/hole-blocking layer/Au electrode.

photocurrent−voltage curves under 100 mW cm^{-2} AM 1.5G simulated irradiation. It was found that the device with a sprayed NiO layer displayed a J_{sc} of 13.54 mA cm^{-2}, an FF of 0.54, and a V_{oc} of 1.01 V, achieving a PCE of 7.39%. The sputtered NiO device presented a J_{sc} of 15.17 mA cm^{-2}, a V_{oc} of 1.1 V, and an FF of 0.59, producing a PCE of 9.84%. The device photovoltaic performance showed a minor difference between the reverse scan and forward scan. As indicated by the histograms in Figure 5c,d, the devices based on sputtered NiO exhibited a better performance than the devices based on sprayed NiO as determined for 21 devices. The PCEs of sprayed-NiO- and sputtered-NiO-based planar devices can be easily pushed to around 7% and 10% (summarized in Table 1). Therefore, the solvent-engineering technology for perovskite formation and a sputtered NiO compact layer are important to obtain $CH_3NH_3PbI_3$ planar devices with high performance and reproducibility. The corresponding incident photon to electron conversion efficiency (IPCE) spectra of champion cells with sprayed NiO and sputtered NiO are depicted in Figure 5b. Compared to the device with sprayed NiO, the device with a sputtered NiO interlayer exhibited higher IPCE values in the range from 400 to 800 nm. The photocurrent integrated from the IPCE spectra gives a current density of 12.94 mA cm^{-2} for the sprayed-NiO-based device and 14.41 mA cm^{-2} for the sputtered-NiO-based device, respectively, which are in agreement with the measured photocurrent density. The IPCE can be expressed as IPCE = $\phi_{inj}\eta_{LHE}\eta_{CC}$, where ϕ_{inj} is the charge injection efficiency, η_{LHE} is the light-harvesting efficiency, and

η_{CC} is the charge collection efficiency. Since the absorption (related to the light-harvesting efficiency) of $CH_3NH_3PbI_3$ films for both devices and the energy level difference (related to the charge injection efficiency) between the charge-carrier-selective layers (i.e., NiO and PCBM layers) and the $CH_3NH_3PbI_3$ film are almost identical (see Figures S2 and S3, Supporting Information), the enhanced IPCE for devices using a sputtered NiO layer could be attributed to an augmented charge collection efficiency. This is correlated with the better interface consistency of sputtered NiO. The shunt resistance (R_{sh}) obtained by fitting the $J-V$ curve with the class diode model was estimated to be much higher for the device with a sputtered NiO layer (57 244 Ω cm^2) than that of the sprayed-NiO-based device (35 860 Ω cm^2), indicating an efficient suppression of interfacial charge recombination at the NiO/$CH_3NH_3PbI_3$ interface.

To further evaluate the role of the blocking layer in this device configuration, the leakage current test was carried out on several devices by reducing the functional layers. As shown in Figure 7, the electron-blocking layer (NiO) and hole-blocking layer (BCP) were certified to forcefully suppress carrier leakage in the interfacial charge transfer process compared with the samples without a blocking layer. Clearly, the sputtered NiO compact layer shows a relatively lower leakage current value than the sprayed NiO layer. A diode-like behavior can be clearly seen for whole devices in the contrast experiment in Figure 7b. The (reverse bias) saturation current density (J_o) of the cell with a BCP layer is significantly lower than that of the device without, thereby leading to a larger open circuit voltage (V_{oc}) of the device with a BCP hole-blocking layer, which is deduced according to the diode equivalent circuit model. All these results illuminate the importance of the EBL and HBL for efficient perovskite planar solar cells and reveal that the sputtered NiO compact layer works very effectively, which is related to comprehensive improvement of the devices.

Electronic IS measurement was further performed to investigate the interfacial charge transfer processes. Figure S4 (Supporting Information) presents the Nyquist plots of the sprayed NiO/$CH_3NH_3PbI_3$(W/O)/PCBM/BCP/Au device and sputtered NiO/$CH_3NH_3PbI_3$(W)/ PCBM/BCP/Au device at a bias of 0.6 V under illumination as an example. The resulting frequency analysis shows two separated semicircles in the Nyquist diagram. In the IS measurements under illumination, when the applied bias (=0.6 V) is less than the open circuit voltage, the photogenerated hole transfers from $CH_3NH_3PbI_3$ to NiO and electrons transfer from $CH_3NH_3PbI_3$ to PCBM and eventually reach the FTO contact. In order of increasing frequency, these arcs are attributed to (i) the charge transfer process at the NiO/$CH_3NH_3PbI_3$ interface in the high frequency range (from 4 MHz to 200 Hz) and (ii) frequency-depended discrete impedance in the low frequency range (from 200 to 0.1 Hz). The impedance response in the low frequency range can be related to $CH_3NH_3^+$ polarization and transportation.[30−32] Figure S4 shows a simplified model for the junction cells based on NiO, including the charge transfer process on the blocking layer interface and charge transport and recombination within the $CH_3NH_3PbI_3$ layer. Figure 8a shows the series resistance (R_s) as a function of the bias. A lower R_s is obtained for the sputtered NiO/$CH_3NH_3PbI_3$(W)/PCBM/BCP/Au device, suggesting that the sputtered NiO interlayer is efficient in charge transportation. The lower R_s might be attributed to the augmented short current and fill factor of this device. Figure 8b presents the recombination resistance (R_{rec})

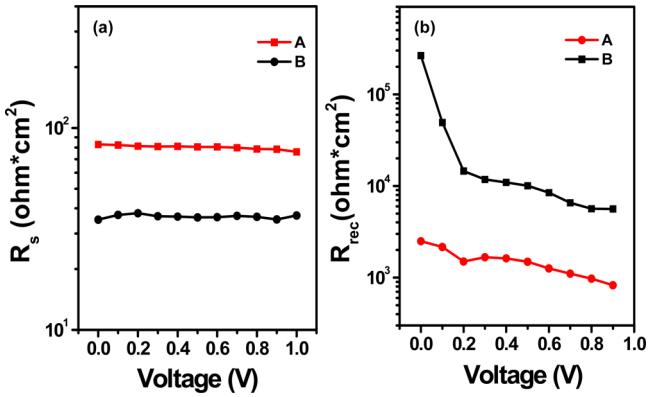

Figure 8. (a) Series resistance (R_s) and (b) charge recombination resistance (R_{rec}) of FTO/sprayed NiO/$CH_3NH_3PbI_3$(W/O)/PCBM/BCP/Au (A) and FTO/sputtered NiO/$CH_3NH_3PbI_3$(W)/ PCBM/BCP/Au (B) from impedance measurements under light. $CH_3NH_3PbI_3$(W) was prepared with the solvent-engineering technology, and $CH_3NH_3PbI_3$(W/O) was prepared without the solvent-engineering process.

for the charge transfer process at the NiO/$CH_3NH_3PbI_3$ interface by fitting the impedance data. It is clear that the sputtered NiO/$CH_3NH_3PbI_3$(W)/PCBM/BCP/Au device displays a larger R_{rec} than the sprayed NiO/$CH_3NH_3PbI_3$(W/O)/PCBM/BCP/Au device, indicating that the interfacial charge recombination process is slower in the former. It is well-accepted that a reduced interfacial recombination could result in an improvement in device photovoltage.[33] Consequently, the IS measurement results suggest that the optimized perovskite layer and sputtered-NiO-selective electrode convincingly improve the device's performance.

CONCLUSION

In conclusion, the sputtered NiO electrode is applied for planar perovskite solar cells. A champion efficiency up to 9.84% has been demonstrated in cooperation with a solvent-engineering perovskite formation method. The underlaid sputtered NiO can efficiently block the NiO/$CH_3NH_3PbI_3$ interlayer electron from recombination, facilitate the formation of uniform surface morphology, and improve the high-class device's reproducibility. In addition, the solvent-engineering $CH_3NH_3PbI_3$ formation method distinctly improved the active layer domains with homogeneous surface coverage and uniform interlayer morphology. The comprehensive information shows us a method to fabricate efficient NiO electrode interlayer/organometallic perovskite planar solar cells and an intuitional insight into the importance of a morphology- and crystallization-compatible interlayer toward a high-performance perovskite solar cell.

ASSOCIATED CONTENT

Supporting Information

Photovoltaic parameters of NiO/$CH_3NH_3PbI_3$/PCBM planar solar cells achieved with different NiO film thicknesses, top-view FE-SEM images of NiO compact layers fabricated on smooth glass, UV−vis results, electronic IS results with fittings, and whole UPS images of the glass/FTO/NiO substrates. This material is available free of charge via the Internet at http://pubs.acs.org.

AUTHOR INFORMATION

Corresponding Authors

*E-mail: huangfeng@nimte.ac.cn.

*E-mail: mingkui.wang@mail.hust.edu.cn.

Notes

The authors declare no competing financial interest.

ACKNOWLEDGMENTS

Financial support from the Director Fund of the Wuhan National Laboratory for Optoelectronics (WNLO), the 973 Program of China (Grants 2014CB643506, 2013CB922104, and 2011CBA00703), the National Natural Science Foundation of China (NSFC) (Grants 21103057, 21161160445, and 21173091), and the Chinise Ministry of Education (CME) with the Program of New Century Excellent Talents in University (Grant NCET-10-0416) is gratefully acknowledged. We thank the Analytical and Testing Centre at the Huazhong University of Science and Technology (HUST) for performing characterization of various samples.

REFERENCES

(1) Zhou, H. P.; Chen, Q.; Li, G.; Luo, S.; Song, T.-B.; Duan, H.-S.; Hong, Z. R.; You, J. B.; Liu, Y. S.; Yang, Y. Interface Engineering of Highly Efficient Perovskite Solar Cells. *Science* **2014**, *345*, 542−546.

(2) Sum, T.-C.; Mathews, N. Advancements in Perovskite Solar Cells: Photophysics behind the Photovoltaics. *Energy Environ. Sci.* **2014**, *7*, 2518−2534.

(3) Xing, G.; Mathews, N.; Sun, S.; Lim, S. S.; Lam, Y. M.; Grätzel, M.; Mhaisalkar, S.; Sum, T. C. Long-Range Balanced Electron- and Hole-Transport Lengths in Organic-Inorganic $CH_3NH_3PbI_3$. *Science* **2013**, *342*, 344−347.

(4) Stranks, S. D.; Eperon, G. E.; Grancini, G.; Menelaou, C.; Alcocer, M. J. P.; Leijtens, T.; Herz, L. M.; Petrozza, A.; Snaith, H. J. Electron-Hole Diffusion Lengths Exceeding 1 Micrometer in an Organometal Trihalide Perovskite Absorber. *Science* **2013**, *342*, 341−344.

(5) Im, J. H.; Lee, C. R.; Lee, J. W.; Park, S. W.; Park, N. G. 6.5% Efficient Perovskite Quantum-Dot-Sensitized Solar Cell. *Nanoscale* **2011**, *3*, 4088−4093.

(6) Burschka, J.; Pellet, N.; Moon, S. J.; Humphry-Baker, R.; Gao, P.; Nazeeruddin, M. K.; Gratzel, M. Sequential Deposition as a Route to High-Performance Perovskite-Sensitized Solar Cells. *Nature* **2013**, *499*, 316−319.

(7) Jeng, J.-Y.; Chiang, Y.-F.; Lee, M.-H.; Peng, S.-R.; Guo, T.-F.; Chen, P.; Wen, T.-C. $CH_3NH_3PbI_3$ Perovskite/Fullerene Planar-Heterojunction Hybrid Solar Cells. *Adv. Mater.* **2013**, *25*, 3727−3732.

(8) Docampo, P.; Ball, J. M.; Darwich, M.; Eperon, G. E.; Snaith, H. J. Efficient Organometal Trihalide Perovskite Planar-Heterojunction Solar Cells on Flexible Polymer Substrates. *Nat. Commun.* **2013**, *4*, 2761−2767.

(9) Sun, S.; Salim, T.; Mathews, N.; Duchamp, M.; Boothroyd, C.; Xing, G.; Sum, T. C.; Lam, Y. M. The Origin of High Efficiency in Low-Temperature Solution-Processable Bilayer Organometal Halide Hybrid Solar Cells. *Energy Environ. Sci.* **2014**, *7*, 399−407.

(10) You, J.; Hong, Z.; Yang, Y.; Chen, Q.; Cai, M.; Song, T.-B.; Chen, C.-C.; Lu, S.; Liu, Y.; Zhou, H.; Yang, Y. Low-Temperature Solution-Processed Perovskite Solar Cells with High Efficiency and Flexibility. *ACS Nano* **2014**, *8*, 1674−1680.

(11) Heo, J. H.; Im, S. H.; Noh, J. H.; Mandal, T. N.; Lim, C.-S.; Chang, J. A.; Lee, Y. H.; Kim, H.; Sarkar, A.; Nazeeruddin, M. K.; Grätzel, M.; Seok, S. I. Efficient Inorganic-Organic Hybrid Heterojunction Solar Cells Containing Perovskite Compound and Polymeric Hole Conductors. *Nat. Photonics* **2013**, *7*, 486−491.

(12) Cai, B.; Xing, Y.; Yang, Z.; Zhang, W.-H.; Qiu, J. High Performance Hybrid Solar Cells Sensitized by Organolead Halide Perovskites. *Energy Environ. Sci.* **2013**, *6*, 1480−1485.

(13) Xiao, Z.; Bi, C.; Shao, Y.; Dong, Q.; Wang, Q.; Yuan, Y.; Wang, C.; Gao, Y.; Huang, J. Efficient, High Yield Perovskite Photovoltaic Devices Grown by Interdiffusion of Solution-Processed Precursor Stacking Layers. *Energy Environ. Sci.* **2014**, *7*, 2619−2623.

(14) Garcia, A.; Welch, G. C.; Ratcliff, E. L.; Ginley, D. S.; Bazan, G. C.; Olson, D. C. Improvement of Interfacial Contacts for New Small-Molecule Bulk-Heterojunction Organic Photovoltaics. *Adv. Mater.* **2012**, *24*, 5368−5373.

(15) Fan, X.; Fang, G.; Cheng, F.; Qin, P.; Huang, H.; Li, Y. Enhanced Performance and Stability in PBDTTT-C-T:PC70BM Polymer Solar Cells by Optimizing Thickness of NiO_x Buffer Layers. *J. Phys. D: Appl. Phys.* **2013**, *46*, 305106−305112.

(16) Manders, J. R.; Tsang, S.-W.; Hartel, M. J.; Lai, T.-H.; Chen, S.; Amb, C. M.; Reynolds, J. R.; So, F. Solution-Processed Nickel Oxide Hole Transport Layers in High Efficiency Polymer Photovoltaic Cells. *Adv. Funct. Mater.* **2013**, *23*, 2993−3001.

(17) Irwin, M. D.; Buchholz, D. B.; Hains, A. W.; Chang, R. P. H.; Marks, T. J. p-Type Semiconducting Nickel Oxide as an Efficiency-Enhancing Anode Interfacial Layer in Polymer Bulk-Heterojunction Solar Cells. *Proc. Natl. Acad. Sci. U.S.A.* **2008**, *105*, 2783−2787.

(18) Jeng, J.-Y.; Chen, K.-C.; Chiang, T.-Y.; Lin, P.-Y.; Tsai, Z.-D.; Chang, Y.-C.; Guo, T.-F.; Chen, P.; Wen, T.-C.; Hsu, Y.-J. Nickel Oxide Electrode Interlayer in $CH_3NH_3PbI_3$ Perovskite/PCBM Planar-Heterojunction Hybrid Solar Cells. *Adv. Mater.* **2014**, *24*, 4107−4113.

(19) Huang, F.; Ge, F.; Zhu, P.; Wang, H.; Meng, F.; Li, S. Superhard V-Si-N Coatings (>50 GPa) with the Cell-like Nanostructure Prepared by Magnetron Sputtering. *Surf. Coat. Technol.* **2013**, *232*, 600−605.

(20) Chan, X.-H.; Jennings, J. R.; Anower Hossain, Md.; Yu, K.-K.-Z.; Wang, Q. Characteristics of p-NiO Thin Films Prepared by Spray Pyrolysis and Their Application in CdS-Sensitized Photocathodes. *J. Electrochem. Soc.* **2011**, *158*, H733−H740.

(21) Lu, J.-F; Xu, X.-B; Cao, K.; Cui, J.; Zhang, Y.-B; Shen, Y.; Shi, X.-B; Liao, S.-H; Cheng, Y.-B; Wang, M.-K. D-π-A Structured Porphyrins for Efficient Dye-Sensitized Solar Cells. *J. Mater. Chem. A* **2013**, *1*, 10008−10015.

(22) Nakaoka, K.; Ueyama, J.; Ogura, K. Semiconductor and Electrochromic Properties of Electrochemically Deposited Nickel Oxide Films. *J. Electroanal. Chem.* **2004**, *571*, 93−99.

(23) Hüfner, S.; Steiner, P.; Sander, I.; Reinert, F.; Schmitt, H. The Electronic Structure of NiO Investigated by Photoemission Spectroscopy. *Solid State Commun.* **1991**, *80*, 869−873.

(24) Greiner, M. T.; Helander, M. G.; Wang, Z.-B.; Tang, W.-M.; Lu, Z.-H. Effects of Processing Conditions on the Work Function and Energy-Level Alignment of NiO Thin Films. *J. Phys. Chem. C* **2010**, *114*, 19777−19781.

(25) Zhai, Z.; Huang, X.; Xu, M.; Yuan, J.; Peng, J.; Ma, W. Greatly Reduced Processing Temperature for a Solution-Processed NiO_x Buffer Layer in Polymer Solar Cells. *Adv. Energy Mater.* **2013**, *3*, 1614−1622.

(26) Uehara, S.; Sumikura, S.; Suzuki, E.; Mori, S. Retardation of Electron Injection at NiO/Dye/Electrolyte Interface by Aluminium Alkoxide Treatment. *Energy Environ. Sci.* **2010**, *3*, 641−644.

(27) Xiao, M. D.; Huang, F. Z.; Huang, W. C.; Dkhissi, Y.; Zhu, Y.; Etheridge, J.; Gray-Weale, A.; Bach, U.; Cheng, Y.-B.; Spiccia, L. A Fast Deposition-Crystallization Procedure for Highly Efficient Lead Iodide Perovskite Thin-Film Solar Cells. *Angew. Chem., Int. Ed.* **2014**, *53*, 1−7.

(28) Huang, F.; Dkhissi, Y.; Huang, W.; Xiao, M.; Benesperi, I.; Rubanov, S.; Zhu, Y.; Lin, X. F.; Jiang, L. C.; Zhou, Y. C.; Gray-Weale, A.; Etheridge, J.; McNeilla, C. R.; Caruso, R. A.; Spiccia, L.; Cheng, Y.-B. Gas-Assisted Preparation of Lead Iodide Perovskite Films Consisting of a Monolayer of Single Crystalline Grains for High Efficiency Planar Solar Cells. *Nano Energy* **2014**, *10*, 10−18.

(29) Jeon, N.-J.; Noh, J.-H.; Kim, Y.-C.; Yang, W.-S.; Ryu, S.; Seok, S. I. Solvent Engineering for High-Performance Inorganic-Organic Hybrid Perovskite Solar Cells. *Nat. Mater.* **2014**, *13*, 897−903.

(30) Kim, H.; Mora-Sero, I.; Gonzalez-Pedro, V.; Fabregat-Santiago, F.; Juarez-Perez, E. J.; Park, N.; Bisquert, J. Mechanism of Carrier Accumulation in Perovskite Thin-Absorber Solar Cells. *Nat. Commun.* **2013**, *4*, 2242−2248.

(31) Gonzalez-Pedro, V.; Juarez-Perez, E. J.; Arsyad, W.; Barea, E. M.; Fabregat-Santiago, F.; Mora-Sero, I.; Bisquert, J. General Working Principles of $CH_3NH_3PbX_3$ Perovskite Solar Cells. *Nano Lett.* **2014**, *14*, 888−893.
(32) Dualeh, A.; Moehl, T.; Tétreault, N.; Teuscher, J.; Gao, P.; Nazeeruddin, M. K.; Grätzel, M. Impedance Spectroscopic Analysis of Lead Iodide Perovskite-Sensitized Solid-State Solar Cells. *ACS Nano* **2014**, *8*, 362−373.
(33) Xu, X.; Zhang, H.; Cao, K.; Cui, J.; Lu, J.; Zeng, X.; Shen, Y.; Wang, M. Lead Methylammonium Triiodide Perovskite-Based Solar Cells: An Interfacial Charge-Transfer Investigation. *ChemSusChem* **2014**, *7*, 3088−3094.